Energy 96 (2016) 644–653

Contents lists available at ScienceDirect

Energy

journal homepage: www.elsevier.com/locate/energy

A control-oriented cycle-life model for hybrid electric vehicle lithium-ion batteries

Girish Suri, Simona Onori*

Department of Automotive Engineering, Clemson University – International Center for Automotive Research, Clemson University, Greenville, SC 29607, USA

ARTICLE INFO

Article history:
Received 28 March 2015
Received in revised form
21 November 2015
Accepted 24 November 2015
Available online 4 February 2016

Keywords:
Optimization
Control-oriented model
Battery
Hybrid electric vehicles

ABSTRACT

In this paper, a semi-empirical Lithium-iron phosphate-graphite battery aging model is identified over data mimicking actual cycling conditions that a hybrid electric vehicle battery encounters under real driving scenarios. The aging model is then used to construct the *severity factor map*, used to characterize relative aging of the battery under different operating conditions. This is used as a battery degradation criterion within a multi-objective optimization problem where battery aging minimization is to be achieved along with fuel consumption minimization. The method proposed is general and can be applied to other battery chemistry as well as different vehicular applications. Finally, simulations conducted using a hybrid electric vehicle simulator show how the two modeling tools developed in this paper, i.e., the severity factor map and the aging model, can be effectively used in a multi-objective optimization problem to predict and control battery degradation.

1. Introduction

Global concerns over pollution and greenhouse gas emissions, increasingly stringent vehicle emission regulations and fluctuating prices of depleting non renewable petroleum resources have encouraged research in sustainable and clean alternatives for modern transportation systems [1]. Hybrid electric vehicles (HEVs) typically have two sources of power, an electric motor and internal combustion engine, and battery and fuel/fuel tank their respective energy storage devices.

The extra degree of freedom offered by the hybrid architecture is exploited to achieve better fuel economy and lower exhaust emissions. Most of the research on energy management strategies design in HEVs has been mainly focused on minimizing fuel consumption under a global constraint of charge sustainability [2]. It is well understood, though, that battery performance significantly affects the long term operation of a hybrid vehicle in terms of expected monetary savings and desired energy efficiency of the powertrain system. The strategies developed and implemented on HEVs thus far have not posed any consideration on extending battery life. Only recently, researchers have started being concerned about battery wear within a vehicle energy management framework [3], and the issue of modeling battery aging for inclusion in a model-based supervisory control has gained more attention [4].

The design, integration, and control of the energy storage system to match the life of a vehicle becomes a new engineering challenge. A possible approach to tackle this challenge can be found in the design of a supervisory control strategy that includes a battery aging model in the minimization function [5].

Mathematically, this can be described as a multi-objective optimization problem aimed at minimizing fuel while ensuring that the battery matches the life of the vehicle. The first formal attempt of investigating the inclusion of battery aging (in terms of capacity degradation) in the energy management problem for HEVs was presented in Ref. [4]. However, the limitation of the approach proposed was in the use of a postulated battery aging model from the manufacturer's datasheet and not from application-driven aging data. A second attempt was presented in Ref. [5], where the authors designed a HEV energy management strategy using the aging model from Ref. [6]. However, this strategy does not predict capacity loss under realistic driving scenarios, and does not include the dependence on one of the main aging factors, *i.e.* state-of-charge (SOC). In Ref. [7], an anode Solid Electrolyte Interface (SEI) layer growth model from Ref. [8] was used to obtain a resistive film growth rate map that was integrated in the optimal control design of power management for a PHEV while including battery aging. Contributions in this area of research are very limited due to the

* Corresponding author.
E-mail addresses: gsuri@clemson.edu (G. Suri), sonori@clemson.edu (S. Onori).

http://dx.doi.org/10.1016/j.energy.2015.11.075
0360-5442/

Nomenclature

Symbols and descriptions

Q_{nom}	Nominal Capacity
V_{oc}	Open Circuit Voltage
R	Internal Resistance
SOC	State of charge
I	current
I_c	Current rate normalized to battery charge capacity
θ	internal temperature
$\overline{SOC}$	Average state of charge
$\overline{I_c}$	Average current rate
$\overline{\theta}$	Average battery internal temperature
Q_{loss}	Normalized capacity loss
Q_{batt}	Remaining battery capacity
p	Vector of severity factors
Ah	Accumulated charge throughput
z	Power law exponent
z^*	Optimum power law exponent
σ_{funct}	Severity factor function
σ^*_{funct}	Optimum severity factor function
σ_{map}	Severity factor map
E_a	Activation energy
R_g	Universal gas constant
α, β, η	Model parameters
ε	Total error
$Q^{data}_{loss,\%,i}$	Capacity loss at the *ith* Ah throughput
$Q^{model}_{loss,\%,i}$	Capacity loss from proposed aging model at the $i-thAh$ throughput
$\bar{z}$	Average power law exponent
R^2	Goodness of fit coefficient
SS_{res}	Residual sum of squares
SS_{tot}	Total sum of squares
EOL	end-of-life
$I_{c,nom}$	Nominal current rate
SOC_{nom}	Nominal state of charge
θ_{nom}	Nominal battery temperature
Γ	Total charge throughput of the battery operated under nominal load cycle
γ	Total charge throughput of the battery operated under a given load cycle
SEI	Solid electrolyte interface
$\frac{\partial \sigma_{map}}{\partial I_c}$	Sensitivity of severity factor map with respect to current rate
$\frac{\partial \sigma_{map}}{\partial \theta}$	Sensitivity of severity factor map with respect to battery internal temperature
$\frac{\partial \sigma_{map}}{\partial SOC}$	Sensitivity of severity factor map with respect to battery state of charge
CVT	Continuous variable transmission
T_{req}	Torque request
T_{em}	Electric machine torque
T_{ice}	Engine torque
T_{br}	Brake torque
T_{CVT}	CVT torque
ω_{em}	Electric machine speed
ω_{ice}	Engine speed
v_{veh}	Vehicle speed
$\dot{m}_f$	Instantaneous fuel consumption rate
P_{batt}	power
u	Control variable
c_a	Transformation coefficient
θ_{amb}	Ambient temperature
Ah_{eff}	Effective charge throughput

lack of formal modeling tools to deal with battery degradation. In order to properly cast a multi-objective optimization problem that accounts for battery life and fuel consumption, a control-oriented battery aging model is needed that is predictive enough for the application under study. In this paper, the life cycle model from Ref. [9] is improved to predict degradation for HEV battery. In particular, the model is validated, for the first time, against Lithium-iron phosphate ($LiFePO_4$)-graphite battery used in the field. In addition, a methodology to design aging degradation maps suited for multi-objective optimization is proposed. HEV batteries undergo frequent charge/discharge cycling which tend to decrease the charge capacity and output power that the battery can deliver [10]. The capacity drop, in general, is due to parasitic side reactions, structural degradations, positive-electrode material dissolution, SEI layer formation and loss of contact between the electrode and the current collector [11]. These batteries usually undergo two different types of aging: cycle life aging and calendar aging. In this paper, only the cycle life aging is considered for which two main families of modeling approaches have been proposed in literature:

- *Electrochemical aging models*: These are physics based models describing the actual phenomena of diffusion [8] and charge transport of ions of lithium inside a battery [12]. The main advantages of these models are their accuracy and their ability to simulate aging under different operating conditions. Their limitations, on the other hand, are in their need for a detailed knowledge of the aging mechanisms and the high CPU time [13]. The integration of these models inside a Battery Management System (BMS) for real time control is currently under research [14].
- *Semi-empirical aging models*: Typically these are phenomenological models developed from data obtained in a laboratory through large scale testing under different aging conditions. Although these models have lower predictability than their electrochemical counterpart as they only describe how the aging mechanisms manifests and do not capture their physics, they are suitable for estimation-control applications as they require low computation time to predict degradation and can be easily integrated within a BMS. In Ref. [6], a semi-empirical aging model was proposed and calibrated over wide temperature and current range (Depth of discharge dependence is neglected in the model); in Ref. [15], a similar model is experimentally validated to predict aging at low SOC of operation at constant temperature; in Ref. [16], an aging model was developed to predict capacity degradation both during discharging and fast charging; a cell degradation study was performed in Ref. [17] that combines driving and vehicle-to-grid (V2G) usage for PHEV batteries; and finally, in Ref. [18], a lifetime prediction model for lithium-ion batteries is validated on profiles defined by the VDA (German association of the automotive industry).

The focus of this paper is on life cycle semi-empirical battery aging models.

This paper is organized in the following way. In Section 2, the identification steps conducted to design the newly calibrated aging model are presented. In Section 3, the derivation of the severity

Table 1
Data for $LiFePO_4$ battery cell (ANR26650) from A123 systems.

Description	Parameter	Value
Nominal Capacity	Q_{nom}	2.5 Ah
Open Circuit Voltage	V_{oc}	3.3 V
Internal Resistance	R	10 mΩ
Cell Weight	m_{cell}	76 g
Cell Diameter	ϕ	26 mm
Cell Height	h	65 mm

factor map from the aging model is illustrated in detail. In Section 4, the emphasis is laid on the sensitivity of the severity factor map with respect to aging parameters. In Section 5, it is shown how the severity factor map is being used in the formulation and development of a multi-objective optimization problem for an HEV for which a description of the vehicle simulator is provided along with simulation results. Conclusions are provided in Section 6.

2. Battery aging model

The cycle life of a battery is usually characterized in a laboratory environment where the battery is subjected to standard/synthetic test profiles that do not necessarily mimic real cycling conditions. In Ref. [6], a three step pulse power characterization profile was used for large scale cycle life experiments of the $LiFePO_4$ (26650) batteries under different constant operating conditions. The aging model proposed in Ref. [6] was identified over these data sets and the dependence on *SOC* neglected. In Ref. [15], square wave current profiles were used to characterize the capacity degradation of the same type of battery used in PHEV applications during a charge sustaining mode at low *SOC*. The aging model was not validated across different temperatures, and capacity loss dependence on temperature was modeled using an Arrhenius-like equation. In Ref. [16], a standardized load profile was used to carry out an experimental aging campaign over a wide range of depth of discharge (*DOD*), temperature and current rate (or C-rate I_c[1]) of operation. Although, the capacity loss behavior was investigated as a function of the above parameters, a comprehensive aging model accounting for all aging factors all together was not provided.

$$I_c = \frac{|I|[A]}{Q_{batt}[Ah]} \tag{1}$$

In this work, the damage accumulation model used to predict battery cycle life ([6] and [19]) is calibrated on battery aging data obtained from a charge sustaining HEV and includes *SOC*, temperature and current rate dependence. The calibration is conducted using graphite-$LiFePO_4$ cells, whose specification is shown in Table 1. The result, shown later in Section 2.1, is a semi-empirical control-oriented aging model that predicts graphite-$LiFePO_4$ battery degradation used in charge-sustained HEVs.

The damage accumulation models proposed of [9] and [6] decouple the effect of the aging factors, *i.e.* current rate, I_c, temperature, θ, and *SOC*, from the accumulated damage expressed in terms of ampere-hour throughput or total number of cycles [20]. With the coherence of this framework, the parameters of the capacity loss model are identified using the data reported in Table 2, where the information for Profile A and B are obtained from Ref. [21] and Profile C is obtained from Ref. [22]. The data of Profile A represents the battery operation in an actual city driving conditions in Gothenburg, Sweden, whereas Profile B illustrates battery

[1] Current rate, I_c or C-rate, with units [1/h], is defined as the ratio of current (I) to the battery capacity (Q_{batt}).

Table 2
Data are specified in terms of average state of charge, $\overline{SOC}$, average C-rate, $\overline{I_c}$, and average battery temperature, $\overline{\theta}$ for both Profiles A and B [21] and Profile C [22].

Data	$\overline{SOC}$ [%]	$\overline{I_c}$ [1/h]	$\overline{\theta}$ [°C]
Profile A	38.5	2.82	36
Profile B	42.0	3.00	38
Profile C	68.0	6.00	45

usage in a load cycle designed over a stochastic process model for HEVs. The data of profile C is an outcome of experimental testing of batteries with load profiles from a real HEV driving cycle. These three profiles are applied to the battery shown in Fig. 1 and are specified in terms of average state of charge, $\overline{SOC}$, average current rate, $\overline{I_c}$ and average battery temperature, $\overline{\theta}$. In this paper, the normalized capacity loss, Q_{loss} [%] is used as a measure of battery degradation:

$$Q_{loss}(p, Ah) = 100 \cdot \frac{Q_{batt}(0) - Q_{batt}(p, Ah)}{Q_{batt}(0)} \tag{2}$$

where p is the vector of aging factors (I_c, θ, SOC) [19], Ah is the accumulated charge throughput, i.e. the total amount of charge that can flow in and out of the battery during its operation, $Q_{batt}(0)$ is the capacity of a new battery that is equal to the nominal battery capacity and $Q_{batt}(p, Ah)$ is the capacity of an aged battery. The functional form of the capacity loss model can be expressed according to [9] as:

$$Q_{loss}(p, Ah) = \sigma_{funct}(p) \cdot Ah^z \tag{3}$$

where z is the power law exponent that represents *Ah* throughput dependence, and $\sigma_{funct}(p)$ is a nonlinear function of severity factors, called the *severity factor function*, that can be expanded as:

$$\sigma_{funct}(p) = (\alpha \cdot SOC + \beta) \cdot \exp\left(\frac{-E_a + \eta \cdot I_c}{R_g \cdot (273.15 + \theta)}\right) \tag{4}$$

where α, β define *SOC* dependence, η models the I_c dependence, R_g is the universal gas constant [23], E_a is the activation energy equal to 31,500 [J mol^{-1}] [6], *SOC* is in fraction and battery temperature, θ is in [°C]. The exponential dependence of σ_{funct} on I_c and θ is similar to [6] while a new linear dependence on *SOC* is introduced in the newly calibrated and extended model. In the next section a procedure to identify the four parameters (z, α, β, η) over the experimental data of Table 2 is presented.

2.1. Parameter identification

In this section a two-step identification procedure for the capacity loss model (3) is presented. A power law dependence on accumulated charge throughput (Ah) and exponential dependence on temperature based on Arrhenius law [6], are assumed. A nonlinear least square-based approach is used to identify model parameters using the experimental data shown in Table 2.

Fig. 1. A123 $LiFePO_4$ cylindrical cell [28].

The MATLAB® nonlinear identification toolbox is used to identify the model parameters by minimizing the total error, ε:

$$\varepsilon = \left[Q_{loss,\%,i}^{data} - Q_{loss,\%,i}^{model}\right]$$
$$\left(z^*, \sigma_{funct}^*\right) = argmin \sum_{i=1}^{n} \left|\varepsilon\right|^2 \quad (5)$$

where $Q_{loss,\%,i}^{data}$ is the capacity loss at the $i-th\ Ah$ throughput, $Q_{loss,\%,i}^{model}$ is the capacity loss obtained from the proposed aging model at $i-th\ Ah$ throughput, and z^* and σ_{funct}^* are the optimal model parameters.

- ***Step 1:*** The identification process is applied over aging model (3) to identify the z and σ_{funct} parameters from the capacity loss data from the three profiles. The values of the parameters for the three load profiles are reported in Table 3. It can be observed that the values of z are close to each other. The average value of z ($= 0.57$) is chosen for further identification of the aging model.
- ***Step 2:*** In this step, the parameters of the severity factor function, namely α, β and η from (4), are identified. In the Q_{loss} model, (3), the average value of power law exponent, $\bar{z}$, identified in step 1 is used:

$$Q_{loss,\%} = (\alpha \cdot SOC + \beta) \cdot \exp\left(\frac{-E_a + \eta \cdot I_c}{R_g \cdot (273.15 + \theta)}\right) \cdot Ah^{\bar{z}} \quad (6)$$

The identified capacity model (6), is shown in Fig. 2 against experimental data points. The optimal values of α and β, are reported in Table 4; for η, a value equal to 152.5 results in the best fitting. The goodness of fit of the identified model to the experimental data is quantified by a coefficient R^2, that is defined as:

$$R^2 = 1 - \frac{SS_{res}}{SS_{tot}} \quad (7)$$

where $SS_{res} = \sum_{i=1}^{n} \varepsilon^2$ is the residual sum of squares and $SS_{tot} = \sum_{i=1}^{n} (Q_{loss,\%,i}^{data} - \overline{Q_{loss,\%}^{data}})^2$ is the total sum of squares [24], and $\overline{Q_{loss,\%}^{data}}$ is the average of the capacity loss data. For each of the load profiles, the identified aging model and the respective R^2 value are reported in Table 5.

2.2. Severity factor function versus severity factor map

The severity factor function characterizes the severity of the aging of a battery under different operating conditions of SOC, I_c, and θ. Given any aging conditions the magnitude of this factor can be greater or less than 1. Its values are different, in general, for different HEV batteries. The severity factor map, σ_{map} [19], characterizes the relative aging of a battery under different operating conditions. It is defined as the ratio of the total accumulated charge throughput (under nominal cycle) to the total charge throughput under actual operating conditions until the end-of-life, EOL, of the battery is reached. From Ref. [19], the severity factor map is given by:

Table 3
Values of z and σ_{funct} in step 1.

Data	z	σ_{funct}
Profile A	0.60	0.0347
Profile B	0.51	0.1000
Profile C	0.60	0.0578

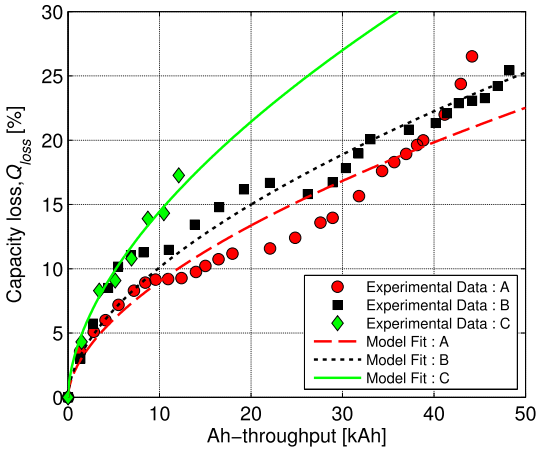

Fig. 2. Curve fitting of identified aging model with the experimental data.

Table 4
Optimal values of α and β.

	$\alpha(SOC)$	$\beta(SOC)$
SOC [%] < 45	2896.6	7411.2
SOC [%] ≥45	2694.5	6022.2

Table 5
Predicted capacity loss for a given profile with R^2.

Data	Aging model	R^2
Profile A	$Q_{loss} = 0.0480 \cdot Ah^{0.57}$	0.9189
Profile B	$Q_{loss} = 0.0530 \cdot Ah^{0.57}$	0.9587
Profile C	$Q_{loss} = 0.0747 \cdot Ah^{0.57}$	0.9798

$$\sigma_{map}(I_c, \theta, SOC) = \frac{\Gamma(I_{c,nom}, \theta_{nom}, SOC_{nom})}{\gamma(I_c, \theta, SOC)} = \frac{\int_0^{EOL} \left|I_{nom}(t)\right| dt}{\int_0^{EOL} \left|I(t)\right| dt} \quad (8)$$

where $\gamma(I_c, \theta, SOC)$ is the total charge throughput of the battery operated under the given pattern of I_c, θ and SOC; while $\Gamma(I_{c,nom}, \theta_{nom}, SOC_{nom})$ is the total charge throughput of the battery operated under nominal load cycle conditions. In this study, $I_{c,nom} = 2.5$ [1/h], $\theta_{nom} = 25\ ^\circ$C, $SOC_{nom} = 35\%$ are chosen as nominal operating conditions under which the battery is assumed to have maximum cycle life. While σ_{funct} can be directly extracted from the data (through identification, as shown in the previous section), the same is not true for σ_{map}. However, it can be obtained and designed from the σ_{funct} itself by means of the procedure presented in the next section.

3. Building severity factor map from aging model

In this section, the design of the severity factor map using the aging model is proposed. The application of this map is particularly suitable for formulating energy management problems (both in HEVs and PHEVs) where battery degradation is a concern. In this paper, the multi-objective optimization framework presented in Section 5 uses the severity factor map as a battery degradation

index. The steps involved in obtaining the map from the aging model are detailed below.

- ***Step 1: Define EOL condition***: Using the aging model in (3), the *EOL* condition when a battery reaches 20% of capacity loss at the nominal operating conditions $(I_{c,nom}, \theta_{nom}, SOC_{nom})$ is defined.

$$20 = \sigma_{funct}(I_{c,nom}, \theta_{nom}, SOC_{nom}) \cdot \Gamma^{\bar{z}} \tag{9}$$

- ***Step 2: Calculating maximum battery life***: The σ_{funct} calculated under nominal operating conditions is used in (9) to calculate the unknown, Γ, that defines the maximum battery life:

$$\Gamma = \left[\frac{20}{\sigma_{funct}(I_{c,nom}, \theta_{nom}, SOC_{nom})}\right]^{1/\bar{z}} \tag{10}$$

The predicted maximum battery life, Γ, obtained from (6) using (10) is equal to 92,342 *Ah*.

- ***Step 3: Battery life under different severity factors***: For a given set of severity factors (I_c, θ, SOC), the estimated value of battery life, defined by γ, is obtained using (9) under the battery *EOL* condition:

$$\gamma = \left[\frac{20}{\sigma_{funct}(I_c, \theta, SOC)}\right]^{1/\bar{z}} \tag{11}$$

The set of γ points can be obtained using different values of severity factors.

- ***Step 4***: ***Creation of*** σ_{map}: Finally, the severity factor map, (8), is a collection of points obtained by taking the ratio of Γ and γ obtained in step 3 and step 4.

The map shown in Fig. 3 is a function of I_c, θ, and *SOC*. It is computed offline for temperatures ranging from $\theta = 10\,^{\circ}C$ to $50\,^{\circ}C$, *SOC* range [20%, 80%], and current rate $I_c = [2C, 20C, 28C]$. The severity factor map plays a similar role of an engine fuel consumption map when used in a model-based optimization framework aimed at minimizing fuel and battery degradation.

The effect of current rate on battery aging weighs more than the effect of temperature and *SOC*. This is shown in Fig. 3, where the curvature of σ_{map} increases significantly with I_c. This implies that the aging of the battery is accelerated under high I_c values. A *high stress zone* and *low stress zone* are defined on the map in order to differentiate between different severity conditions with respect to different degrees of aging.

Temperature has two different effects on the battery's performance [25]. As temperature increases the efficiency of the battery increases due to the decrease in battery's equivalent internal resistance. Simultaneously, it also aggravates battery aging by accelerating the rate of unwanted side reactions, leading to the growth of SEI layer on the electrodes. As shown in Fig. 4, the severity factor map rises with temperature.

Shown in Fig. 5 are the severity factor maps for three different values of *SOC* that almost overlap with each other over the domain of chosen values for I_c and θ. The *SOC* has very little effect on battery degradation.

4. Sensitivity of severity factor map with aging parameters

In this section the relative impact of aging parameters on capacity degradation is presented through a sensitivity study of the severity factor map.

4.1. Sensitivity with respect to current rate, I_c

The sensitivity of the severity factor map with respect to current rate, I_c is defined as:

$$\frac{\partial \sigma_{map}}{\partial I_c} = \frac{1}{z} \cdot \left(\frac{\eta}{R_g}\right) \cdot \frac{\Gamma}{\gamma} \cdot \frac{1}{273.15 + \theta} \tag{12}$$

Fig. 6 shows the sensitivity function (12) with respect to I_c for different values of *SOC* (top figure) and θ (bottom figure). It can be observed that the higher the current rate, the higher is the sensitivity for a given temperature and state of charge. This is due to the exponential dependence of capacity loss on I_c. This suggests that for healthy operation of the battery, it would be advisable to keep the current rate below a certain threshold to avoid accelerated degradation.

4.2. Sensitivity with respect to battery temperature, θ

The sensitivity of the severity factor map with respect to θ is defined as:

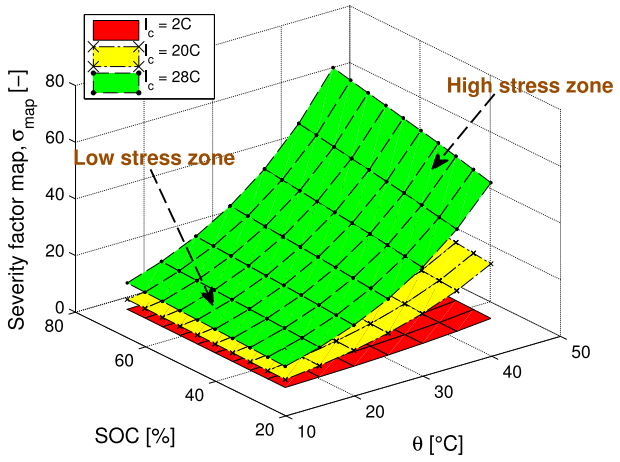

Fig. 3. Severity factor map for three different current rate: I_c = 2C, 20C and 28C.

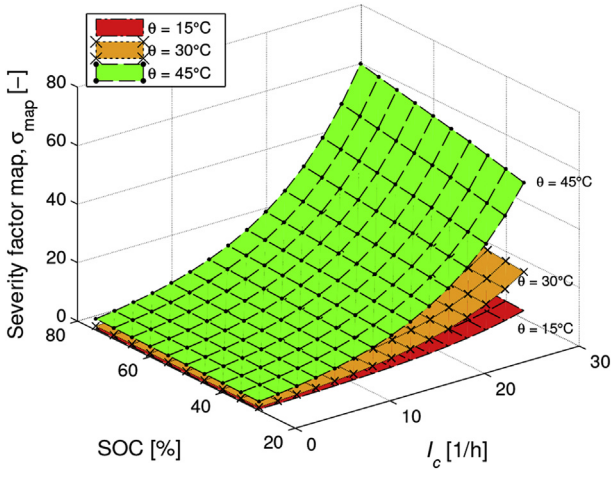

Fig. 4. Severity factor map for three different temperatures: θ = 15 °C, 30 °C and 45 °C.

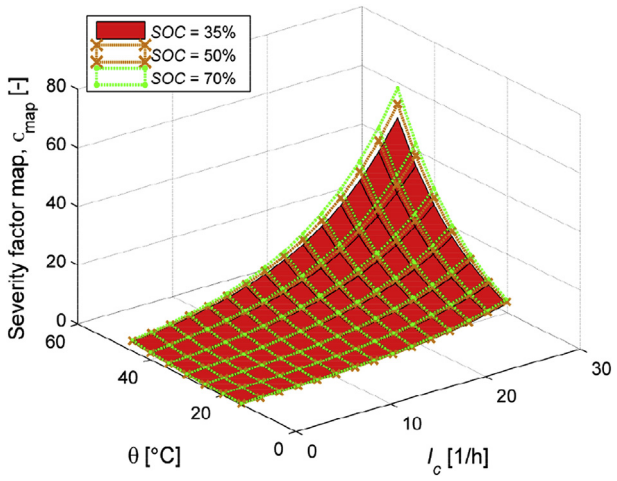

Fig. 5. Severity factor map for three different state of charge: *SOC* = 35%, 50% and 70%.

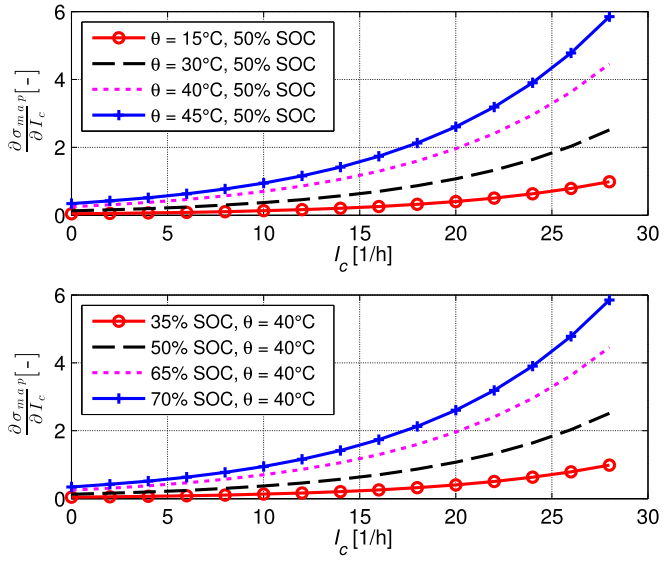

Fig. 6. Sensitivity of severity factor map with respect to I_c with different θ (top) and *SOC* (bottom).

$$\frac{\partial \sigma_{map}}{\partial \theta} = \frac{1}{z}\cdot\frac{\Gamma}{\gamma}\cdot\left[\frac{E_a - \eta\cdot I_c}{R_g}\right]\cdot\frac{1}{(273.15+\theta)^2} \tag{13}$$

From the top plot of Fig. 7 one learns that at a given temperature the magnitude of sensitivity increases with I_c, which is in accordance to the sensitivity trend with respect to I_c shown in Fig. 6. From the bottom plot, it can be noticed that the upward shift of the sensitivity curves is very small for different *SOC* values.

4.3. Sensitivity with respect to state of charge, SOC

Sensitivity of severity factor map with respect to *SOC* is defined as:

$$\frac{\partial \sigma_{map}}{\partial SOC} = \frac{\alpha}{z}\cdot\frac{\Gamma}{\gamma}\cdot\left[\frac{1}{\alpha\cdot SOC+\beta}\right] \tag{14}$$

The trend of σ_{map} over the domain of *SOC* values is almost constant (Fig. 8), which reiterates that *SOC* is not a crucial aging parameter for life estimation of battery in a charge sustaining HEV.

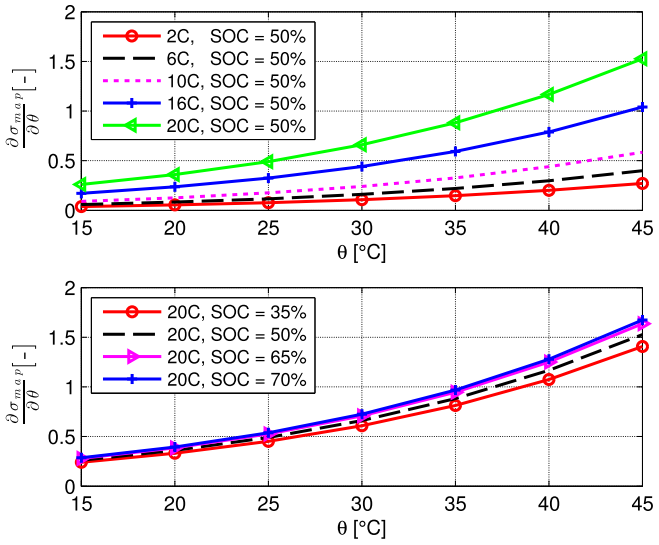

Fig. 7. Sensitivity of severity factor map with respect to θ at *SOC* = 50% (top) and I_c = 20C (bottom).

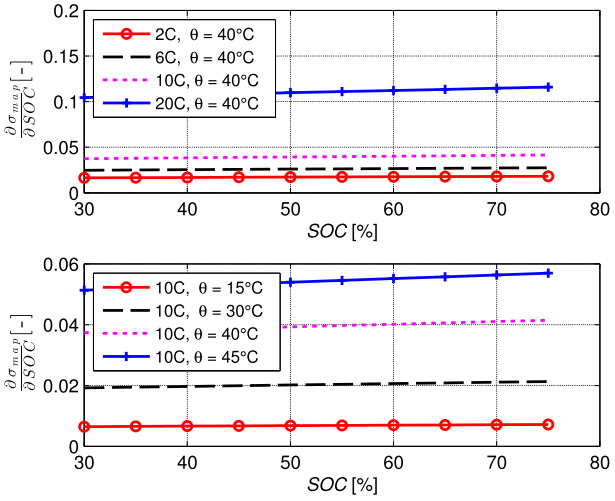

Fig. 8. Sensitivity of Severity factor map with respect to *SOC* at θ = 40 °C (top) and I_c = 10C (bottom).

5. Vehicle simulator layout including battery aging

The main objective of this section is to illustrate the inclusion of a battery aging model in the model-based optimization framework for energy management in a parallel hybrid vehicle. The simulator used in this study, adopted from Ref. [26], is characterized by the information flow shown in Fig. 9. It comprises of the following subsystems:

(i) *Driver model*: The driver is modeled as a simple PID controller that compares the desired vehicle speed (from the drive cycle input) to the actual vehicle speed. Based on the error in the speed, braking and throttle commands are generated from the model such that the vehicle follows the desired speed profile.

(ii) *Energy management strategy*: It is a supervisory controller, which decides how to split the total torque request from the driver, T_{req}, between the electric machine torque, T_{em}, and engine torque, T_{ice}, such that the total torque required is satisfied. The input to the controller are the feedback signals, namely, electric machine speed, ω_{em}, internal combustion

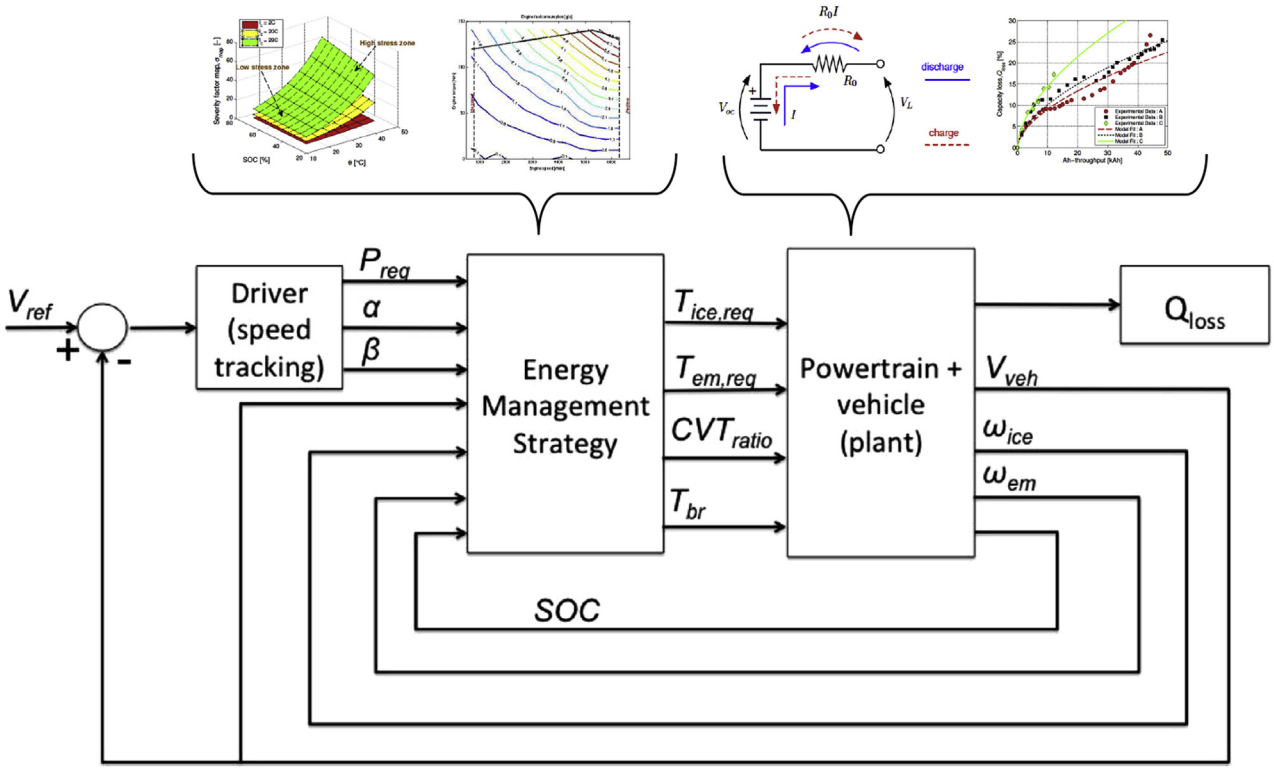

Fig. 9. Layout of HEV simulator used in our study. The battery aging model is used in the Powertrain module to assess the actual state of battery health, whereas the severity factor map is used in the Energy Management Strategy module in a similar manner as the engine fuel consumption map is used. The optimization algorithm interrogates both maps to make the decision as to what the optimal operating points to operate the powertrain are.

engine speed, ω_{ice}, battery *SOC*, current vehicle speed, v_{veh}, both from the powertrain and driver modules. The other controller output is brake torque, T_{br} and CVT torque, T_{CVT}.

(iii) *Powertrain and vehicle model*: The combined model of the HEV powertrain and vehicle comprises various subsystems, such as engine, electric machine, battery pack, battery aging models (i.e., the capacity loss model identified in the previous sections), transmission, brakes, wheels, fuel tank and vehicle dynamics. The details of those subsystems can be found in Ref. [26].

The HEV battery aging model and the severity factor map are both used within the hybrid vehicle simulator to solve the optimal control problem of minimum fuel consumption and minimum battery wear. As shown in Fig. 9, the battery aging model is used in the powertrain module by the BMS (Battery Management System) for state of health estimation, and the severity factor map is instead used in the supervisory controller design, just like an engine map.

The energy management strategy developed in Ref. [4] is applied in this paper. The aim of this strategy is to find the tradeoff between two objectives: minimization of fuel consumption and minimization of battery degradation (through the coefficient $\lambda \in [0,\ 1]$) while respecting HEV charge sustainability constraints at the end of a trip. The objective function is expressed as:

$$J = \int_{t_0}^{t_f} \lambda \cdot \dot{m}_f(u(t)) + (1-\lambda)\cdot\frac{c_a}{\Gamma}\cdot\sigma_{map}(I(u(t)),\theta(t),SOC(t))\cdot\left|I(u(t))\right| dt \qquad (15)$$

where $\dot{m}_f$ is the instantaneous fuel consumption rate [g/s], $u(t) = P_{batt}(t)$ is the control variable, and c_a is a transformation coefficient that makes the amount of battery aging dimensionally compatible with the fuel consumption. In Ref. [4], c_a is defined as a ratio of battery replacement cost to the cost of 1 kg of gasoline; λ is a weighting parameter varying between $[0, 1]$ that gives relative importance to the two costs. To account for battery life usage, the severity factor map, σ_{map} is used in (15). The optimal control problem is solved by the Pontryagin's Minimum Principle (PMP). Details of the PMP algorithm are in the Appendix section.

5.1. Simulation results

Fig. 10 shows the distribution of severity factor map operating points obtained by simulating a FUDS driving cycle at $\theta_{amb} = 30\ ^\circ$C. As FUDS is a mild driving cycle, 64% of the σ_{map} operating points are in the low I_c region (less than 1) which is shown in the inset plot in Fig. 10.

The effect of λ on battery capacity loss simulated over the FUDS cycle is shown in Fig. 11. The top plot shows the evolution of $Q_{loss,\%}$ with respect to time while the bottom plot shows the trend with respect to *Ah*-throughput (or charge throughput). As expected, the capacity loss increases with λ because the cost associated with fuel consumption in (15) increases. As λ increases, the supervisory controller produces a power split such that the proportion of battery power utilized is more than the engine power in the total power request from the driver ($\lambda = 0.5$ defines the situation where the split is the same), resulting into a more pronounced aging of the battery as shown in Fig. 11. This is validated using the Pareto curves shown in Fig. 12, which are obtained over different driving cycles. The fuel consumption difference from the conventional vehicle (condition corresponding to $\lambda = 0$) increases as λ increases, leading

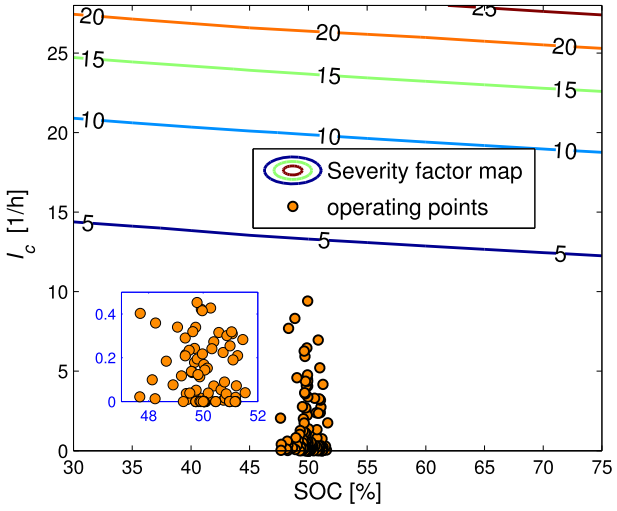

Fig. 10. Distribution of severity factor map operating points at $\theta_{ambient} = 30\ ^{\circ}C$ obtained over FUDS driving cycle.

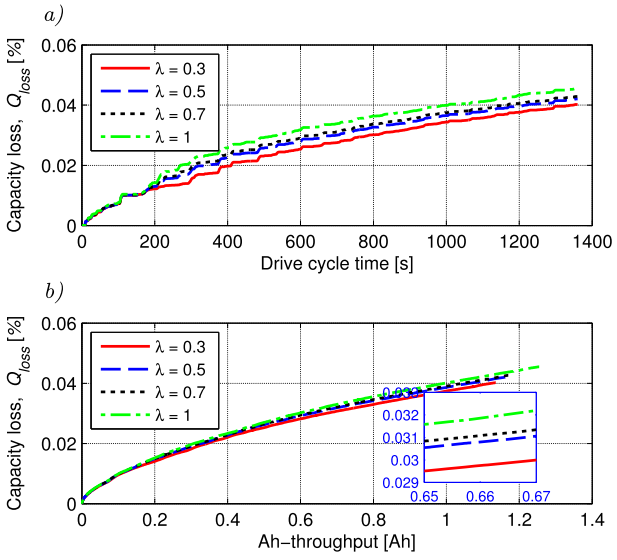

Fig. 11. Q_{loss} over FUDS cycle with different λ a) with respect to time b) with respect to Ah-throughput; at $\theta_{amb} = 30^{\circ}C$

to higher battery degradation. This trend is consistent over different driving cycles.

Shown in Fig. 13 is the comparison of instantaneous variation of current rate over FUDS with different λ. At $\lambda = 1$, battery is subject to higher average values of I_c as the optimizer suggests to use the battery more than the engine, and degradation is not controlled. This, in turn, results in higher battery temperature for $\lambda = 1$ compared to $\lambda = 0.3$, as shown in Fig. 14.

Fig. 15 shows the different *SOC* trends over the FUDS cycle for different values of λ starting from $SOC = 50\%$. The variation of *SOC* is lesser for $\lambda = 0.3$ than $\lambda = 1$, due to lower I_c. In general, though, the maximum difference between *SOC* for these two cases is only about 3% as the sensitivity to *SOC* is much smaller than the sensitivity to I_c and θ, as shown in Fig. 8. As a result, the overall conditions in which the battery operates for $\lambda = 0.3$ are milder than those for $\lambda = 1$.

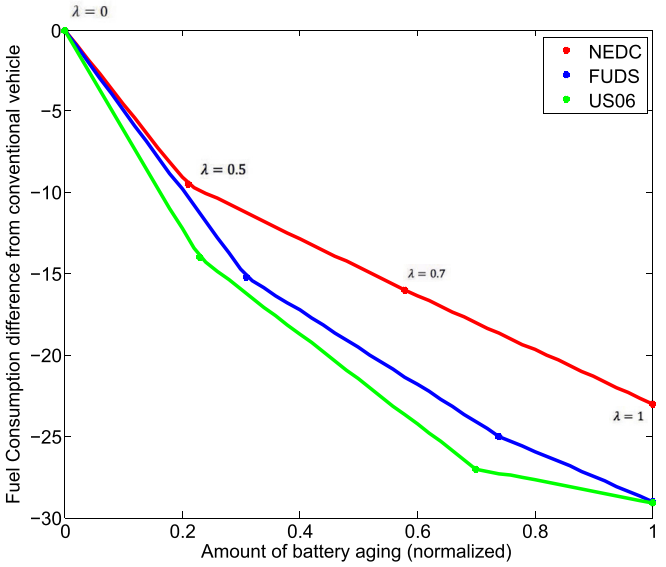

Fig. 12. Pareto curves for different driving cycles – NEDC, FUDS, and US06. Higher amount of aging is obtained as λ increases for all driving cycles.

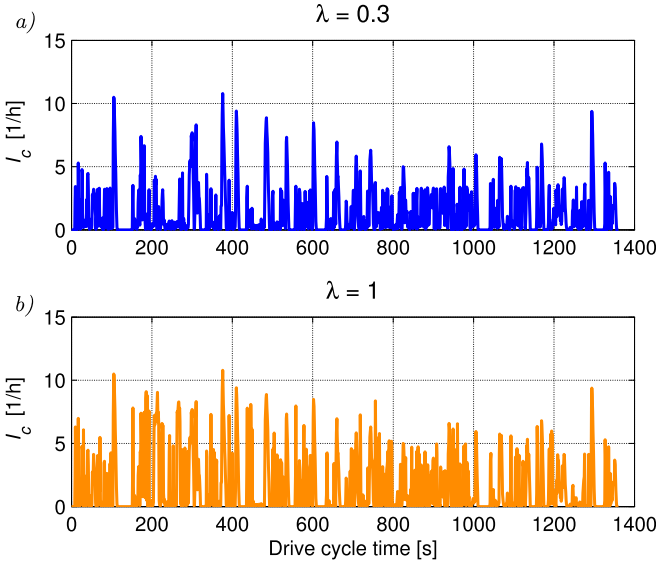

Fig. 13. Current rate over FUDS for a) $\lambda = 0.3$, $\overline{I_c} = 1.3459$; b) $\lambda = 1$, $\overline{I_c} = 1.5243$.

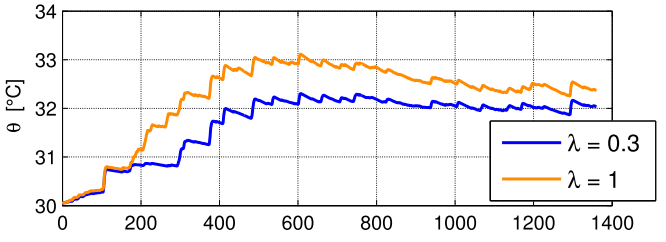

Fig. 14. Battery temperature over FUDS for $\lambda = 0.3$ and $\lambda = 1$.

6. Conclusion

In this paper, a battery capacity degradation model that considers the battery Ah throughput as a measure of battery life is identified over HEV battery data and used to formulate and solve an

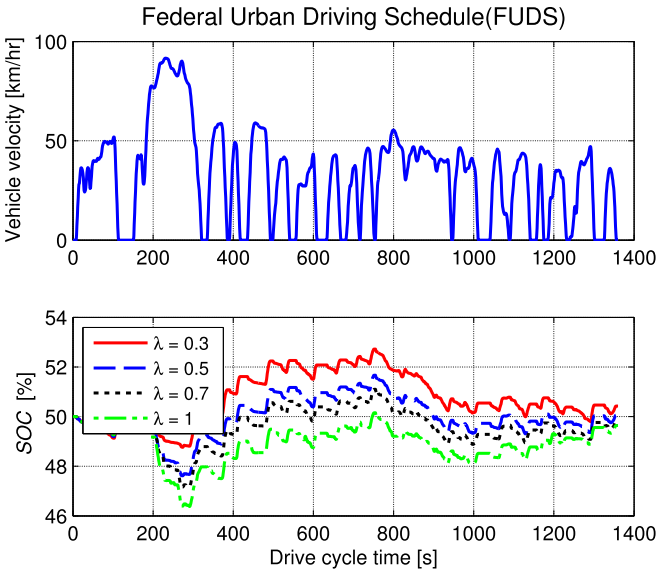

Fig. 15. Velocity profile (top). Variation of *SOC* with λ over FUDS (bottom) at $\theta_{amb} = 30\,^{\circ}$C.

optimal control problem that aims at finding the tradeoff between minimization of battery degradation and fuel consumption. The method to build the severity factor map from the battery aging model is presented, and can be used in a supervisory control setting in the same manner that the engine BSFC map is used. This paper has linked, in a methodical way, the research on battery aging and battery models with a system level optimization. The severity factor map is used as a battery aging index in the multi-objective optimization problem for energy management with consideration of battery aging. The optimal solution provides important insights about the interdependency of battery aging and energy management, and enables the exploration of tradeoff between fuel economy and capacity loss.

Acknowledgment

The authors greatly acknowledge financial support from Honda Research & Development Co., Ltd., under which this work was conducted. We express our special gratitude to Hiroki Tsutsumi and Tetsuaki Nakano for their valuable suggestions in this research.

Appendix

Energy Management using battery aging

In this appendix the formulation of optimal control problem used in this paper and its solution are presented [4].

Problem formulation

The objective of the energy management strategy is to minimize fuel consumption of the vehicle while minimizing the degradation of the battery. In this problem the cost function is expressed as a weighted sum of fuel consumption and battery life, as in (15). While the minimization is performed, the following system dynamics need to be satisfied:

$$\dot{SOC}(u(t), SOC, \theta) = -\eta_{coul}(u(t), \theta)\frac{I(u(t), SOC, \theta)}{Q_{batt}(\theta, t)} \tag{16}$$

where control input $u(t) = P_{batt}(t)$ and η_{coul} is the coloumbic efficiency of the battery. The total power requested at the wheels, $P_{req}(t)$, is an external input whose instantaneous value is known *a priori* [4], and expressed as:

$$P_{req}(t) = P_{ICE}(t) + P_{batt}(t) \tag{17}$$

The local constraints are the physical constraints on the powertrain components, as shown below:

$$\begin{cases} \text{Local constraints}: \\ P_{batt,min} \le P_{batt}(t) \le P_{batt,max} \\ P_{ICE,min} \le P_{ICE}(t) \le P_{ICE,max} \\ P_{mot,min} \le P_{mot}(t) \le P_{mot,max} \end{cases} \qquad \forall t \in \left[t_0, t_f\right] \tag{18}$$

where $(\cdot)_{min}$ and $(\cdot)_{max}$ are the minimum and maximum value of power at each instant of time. The battery power limits are variable because they depend on battery open-circuit voltage, V_{oc}, and internal resistance, R_0. The global constraints on *SOC* are to enforce charge-sustainability, while the local constraints are the boundary limits on the *SOC* profile.

$$\begin{cases} \text{Local constraint}: \quad SOC_{min} \le SOC(t) \le SOC_{max} \\ \text{Global constraint}: \quad SOC(t_0) = SOC\left(t_f\right) = SOC_{ref} \end{cases} \tag{19}$$

where $SOC_{ref} = 50\%$ in this paper, and SOC_{min} and SOC_{max} are the constant minimum and maximum limits for *SOC* (respectively chosen to be 30 and 70%). In addition to local and global constraints, the powertrain constraints are also imposed at each instant such that the total power requested at the wheels is always satisfied, in agreement with the mode of operation.

Optimal Solution

The optimal solution of the aforementioned energy management problem is found by using Pontryagin's Minimum Principle (PMP). The principle states that, in order to minimize *J*, which is a global quantity, the optimal control $u^*(t)$ must minimize instantaneously the Hamiltonian function, *H* defined as[2]:

$$H(u, P_{req}) = \lambda \cdot \dot{m}_f(u, P_{req}) + (1-\lambda)\cdot\frac{c_a}{\Gamma}\cdot\sigma\cdot\left|I\right| + \lambda_{SOC}\cdot\dot{SOC} \tag{20}$$

where λ_{SOC} is the *costate* variable and the system dynamics (i.e., state of charge dynamics) are given in (16). In addition, the dynamics of the costate must be subject to:

$$\begin{aligned} \dot{\lambda}_{SOC} &= -\frac{\partial H}{\partial SOC} \\ &= -\lambda\cdot\frac{\partial \dot{m}_f(u, P_{req})}{\partial SOC} - \frac{(1-\lambda)\cdot c_a}{\Gamma}\cdot\left|I\right|\cdot\frac{\partial\sigma}{\partial SOC} - \lambda_{SOC}\frac{\partial\dot{SOC}}{\partial SOC} \end{aligned} \tag{21}$$

which are dependent on the gradient of the severity factor map with respect to *SOC*. The PMP thus formulated is solved using, for example, the shooting method, that determines the optimal solution by an iterative scheme [27].

References

[1] Chan C. The state of the art of electric and hybrid vehicles. Proc IEEE 2002;90(2):247–75. http://dx.doi.org/10.1109/5.989873.

[2] For simplicity in representing the Hamiltonian function, following variables should be read as $\sigma = \sigma(I_c, \theta, SOC)$, $I = I(u, SOC, \theta)$, $\dot{SOC} = \dot{SOC}(u, SOC, \theta)$.

[2] Guzzella L, Sciarretta A. Vehicle propulsion Systems: Introduction to modeling and optimization. 2007.
[3] L. Serrao, S. Onori, G. Rizzoni, A comparative analysis of energy management strategies for hybrid electric vehicles, J Dyn Syst Meas Control 133(3).
[4] Serrao L, Onori S, Sciarretta A, Guezennec Y, Rizzoni G. Optimal energy management of hybrid electric vehicles including battery aging. In: Proceedings of the 2011 American control Conference; 2011. p. 2125–30.
[5] Ebbesen S, Elbert P, Guzzella L. Battery state-of-health perceptive energy management for hybrid electric vehicles. IEEE Trans Veh Technol 2012;61:2893–900.
[6] Wang J, Liu P, Hicks-Garner J, Sherman E, Soukiazian S, Verbrugge M, et al. Cycle-life model for graphite-$LiFePO_4$ cells. J Power Sources 2011;196:3942–8.
[7] Moura S, Stein J, Fathy H. Battery-health conscious power management in plug-in hybrid electric vehicles via electrochemical modeling and stochastic control. Control Syst Technol IEEE Trans 2013;21(3):679–94.
[8] Ramadass P, Haran B, Gomadam PM, White R, Popov BN. Development of first principles capacity fade model for Li-ion cells. J Electrochem Soc 2004;151(2):A196–203.
[9] Serrao L, Onori S, Rizzoni G, Guezennec Y. A novel model-based algorithm for battery prognosis. In: Proceeding of the 7th IFAC Symposium on fault detection, Supervision and Safety of technical processes. Barcelona: Spain; 2009.
[10] K. Steffke, S. Inguva, D. Cleve, Knockeart J., Accelerated life test methodology for Li-ion batteries in automotive applications.
[11] Safari M, Morcrette M, Teyssot A, Delacourt C. Life-prediction methods for lithium-ion batteries derived from a fatigue approach: II Introduction: capacity-loss prediction based on damage accumulation. J Electrochem Soc 2010;157(6):A713–20.
[12] Safari M, Morcrette M, Teyssot A, Delacourt C. Multimodal physics-based aging model for life prediction of Li-ion batteries. J Electrochem Soc 2009;156(3):A145–53.
[13] Safari M, Delacourt C. Simulation-based analysis of aging phenomena in a commercial graphite/$LiFePO_4$ cell. J Electrochem Soc 2011;158(12):A1436–47.
[14] Prada E, Di Domenico Y, Creff D, Bernard J, Sauvant-Moynot V, Huet F. A simplified electrochemical and thermal aging model of $LiFePO_4$-graphite Li-ion batteries: power and capacity fade simulations,. J Electrochem Soc 2013;4(3):A616–28.
[15] F. Todeschini, S. Onori, G. Rizzoni, An experimentally validated capacity degradation model for Li-ion batteries in phev applications, 8th IFAC International Symposium on fault detection, Supervision and Safety of technical processes.
[16] Omar N, Monem MA, Firouz Y, Salmien J, Smekens J, Hagazy O, et al. Lithium iron phosphate based battery - assessment of aging parameters and development of life cycle model. Appl Energy 2014;113:1575–85.
[17] Whitacre JF, Peterson SB, Apt J. Lithium-ion battery cell degradation resulting from realistic vehicle and vehicle-to-grid utilization. J Power Sources 2010;195(8):2385–92.
[18] Ecker M, Gerschler JB, Vogel J, Kbitz S, Hurst F, Dechent P, et al. Development of a lifetime prediction model for lithium-ion batteries based on extended accelerated aging test data. J Power Sources 2012;215:248–57.
[19] Onori S, Spagnol P, Marano V, Guezennec Y, Rizzoni G. A new life estimation method for lithium-ion batteries in plug-in hybrid electric vehicles applications. Int J Power Electron 2012;4(3):302–19.
[20] Smith K, Neubauer J, Wood E, Jun A, Pesaran M. Models for battery reliability and lifetime applications in design and health management. Ann Arbor, Michigan: Battery Congress; 2013.
[21] J. Groot, State-of-health estimation of Li-ion batteries: cycle life test methods, Licentiate thesis, Energy and Environment, Chalmers University of Technology, Goteborg, Sweden.
[22] P. Spagnol, S. Onori, N. Madella, Y. Guezennec, J. Neal, Aging and characterization of Li-ion batteries in a hev application for lifetime estimation, 6th IFAC Symposium advances on automotive control, Munich Germany.
[23] Rajput R. Engineering thermodynamics: a computer approach (SI Units Version). Infinity science series. Jones & Bartlett Learning; 2010.
[24] Draper N, Smith H. Applied regression analysis. No. pt. 766 in Wiley series in probability and mathematical statistics. Applied probability and statistics. Wiley; 1981.
[25] Smith K, Wang CY. Power and thermal characterization of a lithium-ion battery pack for hybrid-electric vehicles. J Power Sources 2006;160(1):662–73.
[26] Tang L, Onori S, Rizzoni G. Optimal energy management of HEVs with consideration of battery aging. In: 2014 IEEE transportation electrification conference and Expo Beijing, China; 2014.
[27] Serrao L. A comparative analysis of energy management strategies for hybrid electric vehicles (Ph.D. thesis). The Ohio State University; 2009.
[28] A123 $LiFePO_4$ cylindrical cell [Online]. URL http://www.a123systems.com/LiFePO4-battery-cell.htm